energies

MDPI

Article

Physicochemical Properties of Heavy Oil and Emulsification-Controlled Phase Inversion/Stability of Oil–Water Systems

Zhiliang Wang [1], Huiyu Chi [2], Libing Du [3] and Yanfang Feng [1,*]

[1] School of Intelligent Manufacturing, Jingchu University of Technology, Jingmen 448000, China
[2] School of Law, University of International Business and Economics, Beijing 100029, China
[3] School of Geoscience and Technology, Southwest Petroleum University, Chengdu 610500, China
* Correspondence: yanfang111111111@163.com

Abstract

Oil–water emulsions formed by heavy crude oil from Block A of the YT Oilfield during production and transportation are strongly influenced by the oil's high viscosity and density and by its abundant resins and asphaltenes. Such emulsions can increase shear viscosity and flow resistance and may even undergo phase inversion. To clarify these behaviors, the rheology, viscosity–temperature characteristics, density, water cut, and SARA composition of the heavy oil were measured. The effects of emulsification temperature, stirring rate, salinity, and water cut on emulsion phase inversion and stability were then investigated. The oil exhibited weakly non-Newtonian behavior at 0–10 °C and Newtonian behavior at 20–60 °C. Its viscosity at 50 °C was 1323.4 mPa·s, and its density at 20 °C was approximately 0.96 g/cm^3. The water cut was 0.05%, and the combined resin and asphaltene content was about 40%, with resins as the dominant fraction. With increasing water cut, the shear viscosity of the emulsion first rose and then declined, reaching a maximum at the phase inversion point. A higher emulsification temperature shifted the inversion point toward a higher water cut and increased the shear viscosity at inversion. Stirring rate and salinity did not change the position of the inversion point; however, a higher stirring rate increased the shear viscosity at inversion, whereas a higher salinity decreased it. Orthogonal range analysis showed that the factors affecting shear viscosity were ranked as follows: water cut > emulsification temperature > salinity > stirring rate. These findings provide an experimental basis for viscosity reduction, gathering and transportation optimization, and phase inversion control in the YT Oilfield.

Keywords: Block A of YT Oilfield; heavy crude emulsification; phase inversion point; emulsion stability; rheological response; water-cut effect; gathering and transportation

Check for updates

Academic Editor: Hossein Hamidi

Received: 28 September 2026
Revised: 21 October 2026
Accepted: 26 October 2026
Published: 30 October 2026

Copyright: © 2026 by the authors. Licensee MDPI, Basel, Switzerland. This article is an open access article distributed under the terms and conditions of the Creative Commons Attribution (CC BY) license.

1. Introduction

Heavy oil is an unconventional crude oil resource characterized by high viscosity, high density, and high contents of resins and asphaltenes. With the continuous growth of global energy demand and the depletion of conventional crude oil resources, efficient recovery and transportation of heavy oil have become important topics in petroleum engineering. In recent years, extensive studies have been conducted worldwide on the development of unconventional oil and gas resources. Li et al. [1] established a thermal-hydraulic-mechanical (THM) coupled model for enhanced geothermal systems (EGS), revealing the evolution of reservoir seepage and recovery efficiency under multiphysics coupling. Wu et al. [2]

optimized the bottomhole temperature-pressure combination for CO_2 replacement recovery of natural gas hydrates, providing methodological insights for development parameter design of unconventional resources. Feng et al. [3] numerically simulated hydraulic fracture propagation and sensitivity factors under the influence of natural fractures in oil shale reservoirs. Although these studies focused on different types of unconventional resources, their research approaches in reservoir property evaluation, multi-factor coupling analysis, and development parameter optimization provide important methodological references for studying emulsification behavior and phase inversion characteristics of heavy oil emulsion systems.

Heavy oil often coexists with formation water in reservoirs and inevitably experiences mechanical shearing from pumps, valves, and elbows during production. In addition, heavy oil itself contains natural surface-active substances such as resins, asphaltenes, naphthenic acids, and fatty acids, making it highly prone to forming oil–water emulsions [4–6]. Wang et al. [7] used grey relational entropy analysis to study the correlations between heavy oil viscosity and the contents of its polar four components and dipole moment. They found that with increasing resin and asphaltene contents and decreasing oil–water interfacial tension, the water-cut inversion point and temperature inversion point of the emulsion gradually increased. Tian et al. [8] employed heavy oil property testing and re-emulsification experiments to elucidate the formation mechanism of water-in-oil (W/O) emulsions of heavy oil during thermal recovery in the Liaohe Oilfield, identifying external energy inputs (e.g., high-temperature steam, shear, and ultrasound) and the stabilization of the oil–water interfacial film by solid particles (montmorillonite-dominated clay) and natural surfactants (high-resin/asphaltene and high-acid-value fractions) as the primary causes of extensive emulsion formation. Ding et al. [9] reviewed the research progress of emulsifying viscosity reducers for heavy oil and pointed out that emulsification viscosity reduction uses viscosity reducers to emulsify heavy oil into oil-in-water (O/W) emulsions or to convert water-in-oil (W/O) structures into water-in-oil-in-water (W/O/W) structures, thereby reducing heavy oil viscosity and improving the oil–water mobility ratio.

At low water cut, the oil–water system mainly forms W/O emulsions, whose shear viscosity is much higher than that of pure oil, severely reducing gathering and transportation efficiency. When the water cut increases to a critical value, the emulsion undergoes phase inversion from W/O to O/W, and the shear viscosity decreases sharply. This critical water cut is defined as the phase inversion point [10,11]. He et al. [12] investigated two ordinary heavy oils and three extra-heavy oils from the Shengli Oilfield and examined the variations in water-cut inversion point and viscosity enhancement ratio with temperature. The results showed that the water-cut inversion point of heavy oil increased with increasing temperature, and the lower the viscosity of the purified heavy oil, the easier emulsification occurred. Tian et al. [13] found through laboratory experiments that the inversion point of high-viscosity crude oil was lower than that of low-viscosity crude oil. Gong et al. [14] conducted heavy oil–water two-phase flow loop experiments and found that the inversion point of the oil–water mixture tended to occur earlier with increasing mixture flow velocity. Wang et al. [7] experimentally found that with increasing asphaltene and resin contents in heavy oil and decreasing oil–water interfacial tension, the water-cut inversion point of the emulsion gradually increased. In addition, Lin et al. [15] found that the HLB value of heavy oil is closely related to its inversion point. The higher the HLB value of heavy oil, the greater the number of polar functional groups, the stronger the interactions among aggregates, and the more water droplets that can be encapsulated during emulsification with water under the same conditions, thereby increasing the inversion point. Regarding the formation conditions of emulsions, Wang et al. [16] studied the effects of stirring time and stirring rate on W/O emulsions of waxy heavy oil and found that the W/O emulsion tended to stabilize

after stirring for more than 10 min. Chen et al. [17] investigated the effects of stirring rate and time on the droplet size of oil–water emulsions through laboratory experiments and found that with increasing stirring rate, the dispersed-phase droplet size gradually decreased and the stability improved. An et al. [18] studied the effect of emulsification temperature on the stability of W/O emulsions and found that with increasing temperature, the thermal motion of surfactant molecules in crude oil increases, weakening their orderly packing at the oil–water interface. The molecules tend to adopt a more irregular and loosely packed arrangement, and their adsorption/desorption equilibrium shifts toward desorption, so the adsorbed amount on the oil–water interfacial film decreases. This reduces the film thickness, viscoelasticity, and mechanical strength, making it easier for water droplets to coalesce; consequently, the water separation ratio increases and the emulsion stability decreases. Furthermore, salinity, as an important parameter of the aqueous-phase chemical environment, significantly affects the properties of the oil–water interfacial film and emulsion stability [19].

In terms of emulsion stability theory, according to the phase volume fraction theory proposed by Ostwald [20], an oil–water system tends to form a W/O emulsion when the aqueous phase volume fraction is below 25.98%; when the aqueous phase volume fraction is between 25.98% and 74.02%, the oil–water mixture may form either a W/O or O/W emulsion; and when the water cut is above 74.02%, an O/W emulsion is readily formed. According to Stokes' law [21], the phase separation rate of an emulsion is proportional to the oil–water density difference and the square of the droplet radius and inversely proportional to the continuous-phase viscosity. The larger the oil–water density difference and droplet radius, the higher the oil–water separation rate of the emulsion.

Internationally, crude oil emulsions have been extensively studied in recent years. Luo et al. [22] reviewed the progress on emulsification, viscosity, phase inversion characteristics, and prediction methods of crude oil–water mixed systems, emphasizing that the phase inversion point is a crucial parameter for oilfield production and pipeline oil–water mixed transportation. Al-Sakkaf and Onaizi [23] systematically reviewed the effects of emulsification factors—including emulsification method, emulsifier type and concentration, oil type, oil/water ratio, salinity, pH, and temperature—on key emulsion characteristics such as droplet size, interfacial tension, and stability. A systematic review based on PRISMA methodology [24] synthesized the state of the art on the composition and stabilization mechanisms of interfacial material in petroleum emulsions, identifying sulfonates, diprotic acids, phenols, and oxygenated asphaltenes as key interfacially active species. Tang et al. [25] critically reviewed demulsification technologies for oilfield crude oil, providing a rigorous classification and mechanistic analysis of chemical demulsifiers and highlighting current technological gaps in heavy crude processing. At the molecular level, Ma et al. [26] investigated the adsorption behavior and molecular interactions of asphaltene subfractions at the oil–water interface, revealing that interfacially active asphaltenes form protective films that stabilize W/O emulsions. Mahmoudi Alemi and Mohammadi [27] experimentally studied the stability of W/O emulsions induced by asphaltene colloids in heavy oil under atmospheric and high-pressure high-temperature conditions, demonstrating that formation water can reduce asphaltene precipitation and enhance emulsion stability. These international works provide a broader theoretical and methodological context for the present study.

The YT Oilfield is one of the important heavy oil production bases in China, and the heavy oil in its Block A is characterized by high contents of resins and asphaltenes. Existing studies have mostly focused on the influence of a single factor on the viscosity of heavy oil emulsions, lacking systematic correlation analysis between physical properties and emulsification phase inversion behavior. Moreover, studies on the emulsification phase

inversion behavior of heavy oil from Block A of the YT Oilfield under specific operating conditions are rarely reported. In this study, heavy oil from Block A of the YT Oilfield was selected as the research object. First, its rheological curves, constitutive equations, viscosity–temperature curves, density, water cut, and SARA composition were measured according to industry standards to clarify its basic physical properties. Subsequently, without adding surfactants, the effects of emulsification temperature, stirring rate, and salinity on the phase inversion point of oil–water emulsions were investigated, and a four-factor three-level orthogonal experiment was conducted to determine the degree of influence of each factor on the shear viscosity of the emulsions. Finally, single-factor experiments were carried out for the factors with significant effects, and combined with static water separation rate and microstructure analysis, the mechanisms controlling phase inversion and stability of oil–water emulsions were revealed. This study can provide theoretical support for optimizing the process parameters of heavy oil gathering and transportation in the YT Oilfield.

2. Experimental Materials and Methods

2.1. Experimental Materials

The experimental oil sample was heavy oil from Block A of the YT Oilfield. The experimental water included distilled water and produced water from the YT Oilfield. The total salinity of the produced water was 200 g/L, in which the Cl^- concentration was 120 g/L, accounting for 60% of the total salinity; the content of monovalent metal cations such as Na^+ and K^+ was 66 g/L, accounting for 33% of the total salinity; and small amounts of Mg^{2+} and Ca^{2+} were also present. According to the experimental requirements, the produced water and distilled water were mixed at volume ratios of 1:3, 2:2, 3:1, and 4:0 to prepare experimental water with salinities of 50, 100, 150, and 200 g/L, respectively.

2.2. Test Methods for Physical Properties of Heavy Oil

2.2.1. Rheological Properties and Viscosity Tests

The rheological properties of the heavy oil were measured using a Viscotester iQ-Haake viscometer (Thermo Fisher Scientific, Karlsruhe, Germany) equipped with an associated temperature controller. According to SY/T 0520—2008 [28] Determination of Crude Oil Viscosity: Rotational Viscometer Equilibrium Method, 16 mL of oil sample was injected into the rheological test cylinder. The test temperature ranged from 0 to 60 °C at 10 °C intervals. Rheological measurements were performed at shear rates of 0.1–50 s^{-1}. The shear rate of 0 s^{-1} was not used because shear stress is identically zero at zero shear rate. Based on the relationship between shear stress and shear rate, rheological curves were plotted at each temperature, and constitutive equations were fitted. The viscosity at different temperatures was calculated from the constitutive equations, and the viscosity–temperature curve was plotted.

2.2.2. Density Test

According to GB/T 2540—1981 [29] Petroleum Products—Determination of Density (Pyknometer Method), the density of the heavy oil was measured at 20–70 °C (at 10 °C intervals) using a pyknometer and a thermostatic water bath. The density was calculated by Equation (1):

$$\rho_t = \frac{(m_3 - m_1)(\delta - 0.0012)}{m_t} + 0.0012 \quad (1)$$

where m_3 is the mass of the pycnometer containing the sample at t °C, g; m_1 is the mass of the empty pycnometer, g; m_t is the water value of the pycnometer at t °C (i.e., the mass of the pycnometer filled with water at t °C minus the mass of the empty pycnometer), g; δ is the density of water at t °C, g/cm^3, obtained from the appendix of GB/T 2540—1981 Petroleum

Products—Determination of Density (Pyknometer Method); 0.0012 is the density of air at 20 °C and an atmospheric pressure of 760 mmHg, g/cm^3.

2.2.3. Water Content Test

According to GB/T 260—2016 [30] Determination of Water Content in Petroleum Products (Distillation Method), the water content of the heavy oil was determined using a distillation apparatus. The operating procedure was as follows: 50 g of heated heavy oil sample was added to a cleaned round-bottom distillation flask, followed by the addition of 100 mL of xylene. After shaking uniformly, boiling chips were added. After the apparatus was connected, the voltage was first adjusted to 50 V for preheating for 30 min, and then increased until liquid dripped from the slanted outlet of the condenser at a rate of 2–4 drops per second. Heating was continued until the volume of water in the receiver no longer increased, and the volume of water at the bottom of the receiver was read. The water content was calculated by Equation (2):

$$\theta = \frac{v\rho}{m} \times 100\% \quad (2)$$

where v is the volume of water obtained by distillation, mL; ρ is the density of water, taken as 1 g/cm^3; m is the mass of the heavy oil, g; θ is the water content of the oil, %.

2.2.4. SARA Analysis

According to NB/SH/T 0509—2010 [31], Determination of Four Fractions in Petroleum Asphalt, the mass fractions of saturates, aromatics, resins, and asphaltenes in the heavy oil were analyzed using a four-component analyzer. The operating procedure was as follows: asphaltenes in the oil sample were first precipitated with n-heptane and filtered, and the precipitate was then reflux-washed with n-heptane to remove entrained soluble components. Toluene was added under reflux to dissolve the asphaltenes; after toluene was evaporated to dryness, the mass fraction of asphaltenes was obtained. The deasphaltened oil sample was adsorbed on an alumina chromatographic column and sequentially eluted with n-heptane, toluene, and toluene–ethanol to obtain the mass fractions of saturates, aromatics, and resins, respectively.

2.3. Preparation of Oil–Water Emulsions and Determination of Phase Inversion Point

Heavy oil from Block A of the YT Oilfield was mixed with experimental water at different water cuts and emulsified for 5 min at a preset emulsification temperature and stirring rate to prepare oil–water emulsions. The shear viscosity of the emulsions at 50 °C was measured using a Viscotester iQ-Haake viscometer, and the relationship curve between shear viscosity and water cut was plotted. The water cut corresponding to the peak shear viscosity was defined as the phase inversion point. Meanwhile, the water separation ratio of the emulsions after standing for 3 h was measured using colorimetric tubes, with measurements taken at 0.5 h intervals. The microstructure of the emulsions was observed using an XPF-550 polarizing microscope (Shanghai Caikon Optical Instrument Co., Ltd., Shanghai, China).

All emulsion preparation, viscosity measurement, and water-separation tests were performed in triplicate. The results presented in all figures are mean values of these triplicate measurements. Error bars are not shown in the figures for clarity; the replicate number, RSD values, and statistical methods are summarized in Appendix Table A1. Statistical analysis was performed using one-way ANOVA followed by Tukey's test ($p < 0.05$).

2.4. Orthogonal Experimental Design

To analyze the degree of influence of different emulsification factors on the shear viscosity of the emulsions, four factors—water cut, emulsification temperature, stirring rate,

and salinity—were selected to conduct a four-factor, three-level orthogonal experiment. The factor-level table is shown in Table 1, and the L9(3^4) orthogonal array is shown in Table 2. With the shear viscosity of the emulsion as the evaluation index, the K value, k value, and range R of each factor were calculated to determine the order of influence.

Table 1. Factor and level table.

Factor	Water Cut (%)	Emulsification Temperature (°C)	Stirring Rate (rpm)	Salinity (g/L)
Level 1	20	30	500	40
Level 2	40	50	750	80
Level 3	60	70	1000	120

Table 2. L9(3^4) orthogonal array.

No.	Water Cut (%)	Emulsification Temperature (°C)	Stirring Rate (rpm)	Salinity (g/L)
1	20	30	500	40
2	20	50	1000	80
3	20	70	750	120
4	40	30	1000	120
5	40	50	750	40
6	40	70	500	80
7	60	30	750	80
8	60	50	500	120
9	60	70	1000	40

3. Results and Discussion

3.1. Physical Properties of Heavy Oil

3.1.1. Rheological Properties and Constitutive Equations

Figure 1 shows the rheological curves of heavy oil from Block A of the YT Oilfield at 0–60 °C and shear rates of 0–50 s^{-1}. As shown in Figure 1, as the test temperature increased from 0 °C to 60 °C, the rheological curves gradually changed from steep to flat, indicating that the rheological properties of the oil sample were relatively sensitive to temperature changes. Within the range of 0–60 °C, the shear stress varied approximately linearly with shear rate, but the degree of nonlinearity was relatively significant at low temperatures.

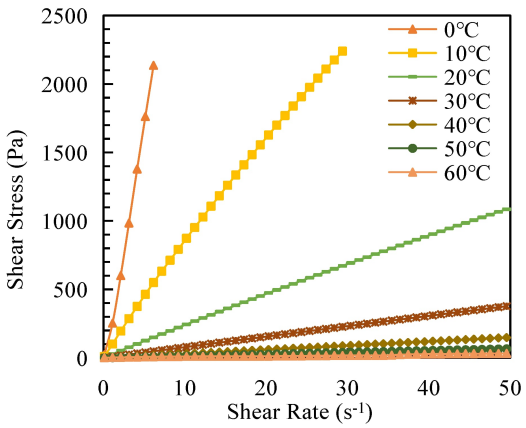


Figure 1. Rheological curves of heavy oil from Block A of the YT Oilfield at 0–60 °C.

The constitutive equations fitted from the rheological curves are listed in Table 3. As can be seen from Table 3, the heavy oil from Block A of the YT Oilfield exhibited power-

law fluid characteristics at 0–10 °C, but the flow behavior index was close to 1, indicating weak non-Newtonian behavior. At 0 °C, the flow behavior index was slightly greater than 1, showing slight dilatant behavior; at 10 °C, it was slightly less than 1, indicating pseudoplastic behavior; at 20–60 °C, the flow behavior index was 1, and the oil sample behaved as a Newtonian fluid. With increasing temperature, the consistency coefficient in the constitutive equation decreased continuously. The fitting correlation coefficients R^2 at all temperatures were above 0.9, indicating that the constitutive equations were highly reliable.

Table 3. Constitutive equations of heavy oil from Block A of the YT Oilfield at 0–60 °C.

Test Temperature (°C)	Constitutive Equation	Correlation Coefficient (R^2)
0	$\tau = 269.25\dot{\gamma}^{1.1202}$	0.9971
10	$\tau = 92.627\dot{\gamma}^{0.9559}$	0.9992
20	$\tau = 22.492\dot{\gamma}$	0.9980
30	$\tau = 7.6797\dot{\gamma}$	0.9998
40	$\tau = 2.9962\dot{\gamma}$	1.0000
50	$\tau = 1.3234\dot{\gamma}$	1.0000
60	$\tau = 0.6487\dot{\gamma}$	0.9308

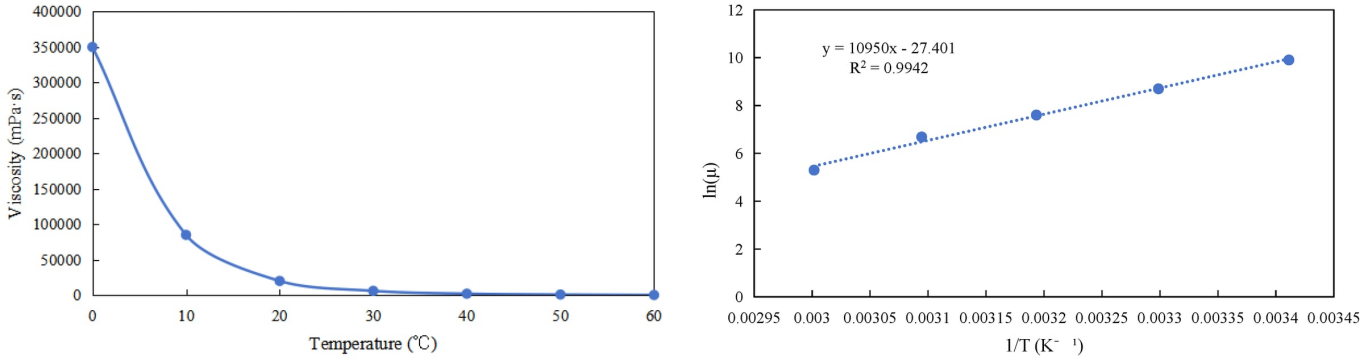
At low temperatures, polar functional groups in resin and asphaltene molecules can form intermolecular hydrogen bonds and van der Waals interactions between resin–resin, asphaltene–asphaltene, and resin–asphaltene aggregates. These interactions promote association and cause weak non-Newtonian behavior. As temperature increases, thermal motion disrupts these interactions, and the oil gradually approaches Newtonian behavior. This interpretation is consistent with previous studies on heavy-oil aggregation and interfacial activity [7,26,27]. As the temperature increases, molecular thermal motion intensifies, the association structure dissociates, and the oil sample gradually behaves as a Newtonian fluid. The flow behavior index was 1 above 20 °C, indicating Newtonian behavior; that is, the shear viscosity was independent of shear rate in this temperature range.

3.1.2. Viscosity–Temperature Characteristics

The viscosity–temperature data are shown in Figure 2. The viscosity decreases monotonically with increasing temperature. For the weakly non-Newtonian data at 0 and 10 °C, the viscosities were calculated from the fitted constitutive equations at a fixed shear rate of 0.1 s^{-1}; these data are reported only as engineering viscosity values and were not used for Arrhenius analysis. In the Newtonian region (20–60 °C), the temperature dependence of viscosity was analyzed using the Arrhenius equation:

$$\ln\ \mu = \ln\ A + \frac{E_a}{RT} \tag{3}$$

where μ is the viscosity (mPa·s), A is the pre-exponential factor, Ea is the apparent activation energy for viscous flow (J·mol^{-1}), R is the gas constant, and T is the absolute temperature (K). The fitted result is $\ln\mu = 10{,}949/T - 27.40$ with $R^2 = 0.994$, corresponding to Ea ≈ 91.0 kJ/mol. This value characterizes the overall temperature sensitivity of viscous flow in the Newtonian region. The 0–10 °C data are weakly non-Newtonian and were therefore not included in the Arrhenius fit, because the apparent viscosity at a fixed shear rate is not a true material viscosity; they are reported only as engineering viscosity data.



(**a**) (**b**)

Figure 2. Viscosity–temperature characteristics of heavy oil from Block A of the YT Oilfield. (**a**) Linear μ–T representation (0–60 °C) for engineering visualization only; (**b**) Arrhenius fit of lnμ versus 1/T strictly for the Newtonian region (20–60 °C).

3.1.3. Density–Temperature Relationship

The density of heavy oil from Block A of the YT Oilfield was measured at 20–70 °C, and the results are listed in Table 4. Based on Table 4, the density–temperature relationship curve was plotted, as shown in Figure 3. The fitted equation for the variation in density with temperature is shown in Equation (4):

$$\rho_t = -1.1 \times 10^{-3} T + 0.9898 \quad (4)$$

with $R^2 = 0.9794$, indicating that it can reasonably predict the density of the heavy oil at 20–70 °C. As shown in Figure 3, the density of the heavy oil decreased with increasing temperature. Except for a slightly lower density value at 20 °C, the overall relationship showed reasonable linearity. The density of the heavy oil at 20 °C was approximately 0.96 g/cm^3. The decrease in density with increasing temperature is consistent with the general law of thermal expansion of liquids. The relatively high density of the heavy oil is related to its high content of heavy components. The linear density–temperature relationship can be used for volume and mass conversion of oil and process calculations during gathering and transportation.

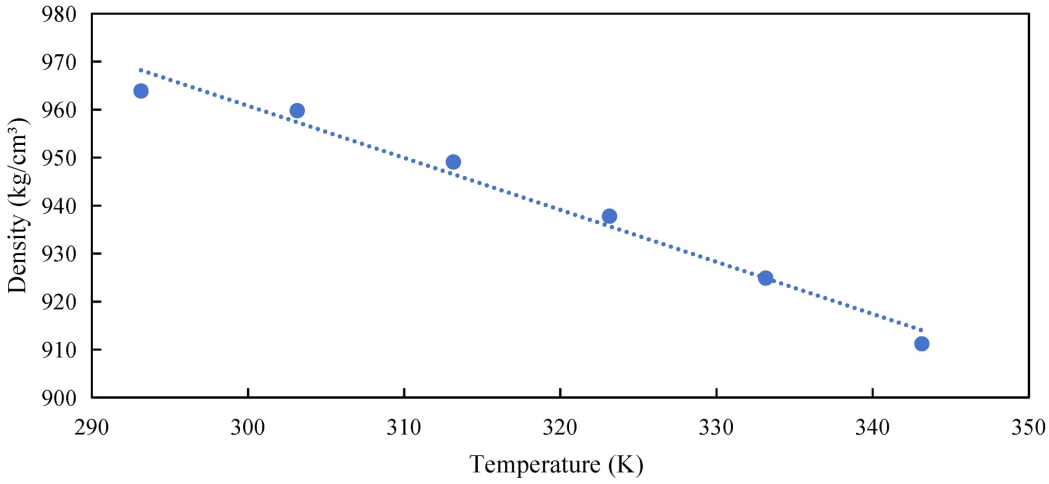


Figure 3. Density–temperature relationship curve of heavy oil from Block A of the YT Oilfield (20–70 °C).

Table 4. Density of heavy oil from Block A of the YT Oilfield (20–70 °C).

Temperature (°C)	20	30	40	50	60	70
Density (g/cm³)	0.9639	0.9598	0.9491	0.9378	0.9249	0.9112

3.1.4. Water Content

The water content of heavy oil from Block A of the YT Oilfield was measured three times, and the results are listed in Table 5. The water volumes collected in the receiver for the three measurements were 0.030, 0.025, and 0.020 mL, respectively. According to Equation (2), the calculated water contents were 0.06%, 0.05%, and 0.04%, with an arithmetic mean of 0.05%. The water content was extremely low; therefore, the heavy oil can be regarded as anhydrous pure oil. This provides a basis for the subsequent oil–water emulsification experiments: the aqueous phase in the experimental emulsions mainly came from externally added mineralized water rather than water inherently carried by the heavy oil.

Table 5. Water content determination of heavy oil from Block A of the YT Oilfield.

Parameter	**First**	**Second**	**Third**	**Average Water Content (%)**
Mass weighed (g)	50	50	50	0.05
Water volume (mL)	0.030	0.025	0.020	
Measured water content (%)	0.06	0.05	0.04	

3.1.5. SARA Composition and Its Influence on Emulsification

The SARA analysis results of heavy oil from Block A of the YT Oilfield are listed in Table 6. As can be seen from Table 6, the heavy oil contained 29.83% aromatics, 24.94% resins, 14.43% asphaltenes, and 30.32% saturates. The total content of resins and asphaltenes was approximately 40%, with a relatively high resin content and a relatively low asphaltene content. Asphaltenes are macromolecular substances containing numerous fused-ring aromatic hydrocarbons, which, after interacting with resins, are dispersed in the light components of heavy oil in the form of colloidal particles. Resins are yellowish-brown viscous colloidal macromolecular organic substances with strong polarity. As natural surfactants with relatively high lipophilicity, they readily cause heavy oil to form W/O emulsions. Resin molecules themselves contain carboxylic acid and aldehyde/ketone groups, which make crude oil more viscous. The interaction between resins and asphaltenes can form high-strength hydrogen bonds, greatly increasing intermolecular forces and thereby significantly enhancing heavy oil viscosity. Therefore, the high contents of resins and asphaltenes in heavy oil from Block A of the YT Oilfield are important intrinsic reasons for its tendency to form stable W/O emulsions and its relatively high phase inversion point.

Table 6. Component contents of heavy oil from Block A of the YT Oilfield.

Aromatics (wt%)	**Resins (wt%)**	**Asphaltenes (wt%)**	**Saturates (wt%)**
29.83	24.94	14.43	30.32

3.2. Factors Influencing Phase Inversion and Stability of Oil–Water Emulsions

Heavy oil production is often accompanied by the production of formation water and is subjected to mechanical stirring from elbows, valves, and pumps during pipeline transportation. In addition, heavy oil itself contains natural surfactants, making it prone to forming oil–water emulsions. At low water cut, the oil–water system forms a highly viscous

W/O emulsion under mechanical stirring, which reduces production and transportation efficiency and may even damage gathering and transportation equipment. As the water cut increases, the water droplets dispersed in the heavy oil rapidly increase, the oil–water interfacial interaction is enhanced, and the shear viscosity gradually increases, reaching a peak at a certain point. With a further increase in water cut, the contact area of the oil–water interfacial film expands and the film becomes thinner. The heavy oil can no longer completely encapsulate the fine water droplets, and free water is ultimately separated out, resulting in inversion to an O/W emulsion and a decrease in shear viscosity. The water cut corresponding to the peak shear viscosity is defined as the phase inversion point. Understanding the phase inversion point and stability behavior is of great significance for heavy oil production and transportation.

3.2.1. Effect of Emulsification Temperature on the Phase Inversion Point

Heavy oil from Block A of the YT Oilfield and produced water from the YT Oilfield were used to prepare oil–water emulsions at different water cuts and emulsification temperatures of 30, 50, and 70 °C, with a stirring rate of 750 rpm and an emulsification time of 5 min. The shear viscosity of the emulsions at 50 °C was measured, and the results are shown in Figure 4. A comparison of different emulsification temperatures shows that with increasing emulsification temperature, the phase inversion point of the emulsion shifted to a higher water cut, and the shear viscosity at the phase inversion point increased.

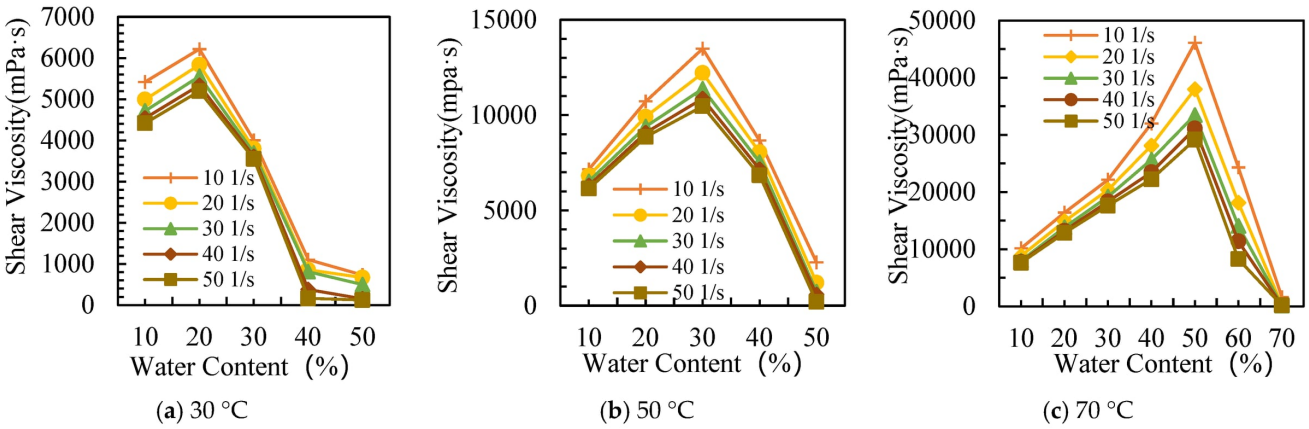


Figure 4. Variation in shear viscosity of heavy oil emulsions from Block A of the YT Oilfield with water cut at different emulsification temperatures.

The emulsions were prepared at water cuts increasing in 10% increments. Therefore, the reported phase inversion point has a resolution/uncertainty of ±10%, and the true inversion point lies between the adjacent water cuts. More closely spaced water-cut experiments near the inversion point will be considered in future work.

At an emulsification temperature of 30 °C, the shear viscosity of the emulsion increased when the water cut increased from 10% to 20%. After the water cut exceeded 20%, the shear viscosity continuously decreased. The phase inversion point was 20%, and the shear viscosity at the phase inversion point was 5000–6000 mPa·s. When the emulsification temperature was increased to 50 °C, the shear viscosity continuously increased as the water cut increased from 10% to 30%. When the water cut increased from 30% to 50%, the shear viscosity continuously decreased. The phase inversion point shifted from 20% to 30%, and the shear viscosity at the phase inversion point increased significantly to 10,000–14,000 mPa·s. When the emulsification temperature was increased to 70 °C, the phase inversion point shifted to 50%, and the shear viscosity at the phase inversion point increased to 30,000–50,000 mPa·s.

The phase inversion point increased with increasing emulsification temperature because the increase in temperature significantly reduced the viscosity of the heavy oil. At the same stirring rate, the surface-active substances in the heavy oil were more fully dispersed in the light components and had higher solubility. The adsorption amount of the associates formed by the active components at the oil–water interfacial film increased, and the viscoelasticity and stability of the oil–water interfacial film were significantly enhanced. Under a given mechanical stirring condition, the heavy oil could encapsulate more small water droplet aggregates, and the oil–water contact area increased. Therefore, the higher the emulsification temperature, the larger the phase inversion point of the emulsion and the higher the shear viscosity at the phase inversion point.

3.2.2. Effect of Stirring Rate on the Phase Inversion Point

With the emulsification temperature controlled at 50 °C and the emulsification time at 5 min, heavy oil from Block A of the YT Oilfield and produced water from the YT Oilfield were used to prepare emulsions at different water cuts under stirring rates of 250, 500, 750, 1000, and 1250 r/min. The shear viscosity at 50 °C was measured, and the relationship between shear viscosity and water cut at a shear rate of 20 s^{-1} was plotted, as shown in Figure 5.

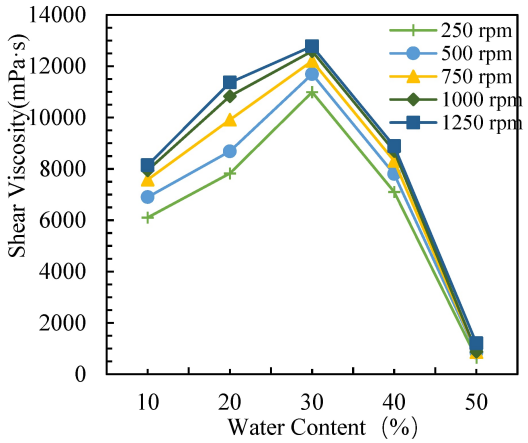


Figure 5. Variation in shear viscosity of heavy oil emulsions from Block A of the YT Oilfield with water cut at different stirring rates.

As can be seen from Figure 5, the variation trends of the shear viscosity of the emulsions with water cut were similar at different stirring rates: when the water cut was 10–30%, the shear viscosity increased with increasing water cut; after the water cut exceeded 30%, the shear viscosity decreased significantly. The phase inversion point of the emulsions was 30% at all stirring rates, indicating that the stirring rate did not change the position of the phase inversion point. However, the shear viscosity at the phase inversion point increased with increasing stirring rate. Within 250–1250 r/min, as the stirring rate increased, the shear viscosity at the phase inversion point increased from 10,990.3 mPa·s to 12,776.8 mPa·s.

The reasons why the shear viscosity at the phase inversion point increased with increasing stirring rate are as follows. First, at the phase inversion point, the W/O emulsion had already undergone emulsification to the greatest extent, and the number of small water droplets encapsulated in the heavy oil reached its limit. Increasing the stirring rate caused the water droplets dispersed in the heavy oil to be cut into finer fragments and distributed more densely in the oil phase. The contact area of the oil–water interfacial film increased, and the van der Waals forces between droplets during flow were enhanced. Therefore, the higher the stirring intensity, the higher the shear viscosity at the phase inversion point. Second, a higher stirring rate produced finer water droplets and a denser droplet population,

as observed by microscopy. This increased droplet–droplet interaction and interfacial area, thereby increasing the shear viscosity at the phase inversion point. This interpretation is consistent with published studies on droplet breakup and emulsion stability [17,23].

3.2.3. Effect of Salinity on the Phase Inversion Point

Produced water from the YT Oilfield and distilled water were mixed at different ratios to prepare experimental water with salinities of 50, 100, 150, and 200 g/L. Emulsions were prepared with heavy oil from Block A of the YT Oilfield at different water cuts. The emulsification temperature was controlled at 50 °C, the stirring rate at 750 r/min, and the emulsification time at 5 min. The shear viscosity at 50 °C was measured, and the relationship between shear viscosity and water cut at a shear rate of 20 s^{-1} was plotted, as shown in Figure 6.

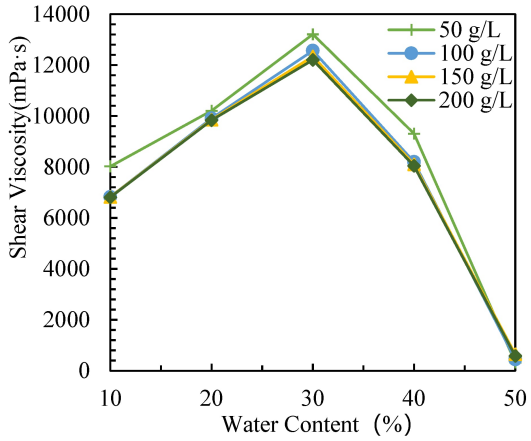


Figure 6. Variation in shear viscosity of heavy oil emulsions from Block A of the YT Oilfield with water cut at different salinities.

As can be seen from Figure 6, the variation trends of the shear viscosity of the emulsions with water cut were similar at different salinities: when the water cut was 10–30%, the shear viscosity increased with increasing water cut; after the water cut exceeded 30%, the shear viscosity decreased significantly. The phase inversion point of the emulsions was 30% at all salinities, indicating that salinity did not change the position of the phase inversion point. As the salinity increased from 50 g/L to 200 g/L, the shear viscosity at the phase inversion point showed a gradually decreasing trend, but the overall change was not large.

The decrease in shear viscosity at the inversion point with increasing salinity may be attributed to compression of the electrical double layer, ionic interference with the oil–water interfacial film, and possible formation of metal soaps from Na^+/K^+ and natural acidic components. These effects can weaken the interfacial film, promote coalescence, and facilitate free-water separation. This interpretation is supported by previous studies on salt effects in heavy-oil emulsions [19,27].

3.2.4. Range Analysis of Orthogonal Experiments

To analyze the degree of influence of different emulsification factors on the shear viscosity of the emulsions, four factors—water cut, emulsification temperature, stirring rate, and salinity—were selected to conduct a four-factor, three-level orthogonal experiment. The $L9(3^4)$ orthogonal array is shown in Table 7. In the table, K1, K2, and K3 are the sums of the experimental data at levels 1, 2, and 3 for a given factor, respectively; k1, k2, and k3 are the averages of K1, K2, and K3, respectively; and R is the range, equal to the difference between the maximum and minimum values of k1, k2, and k3 for the same factor. A larger range indicates a greater fluctuation in the data when the factor takes different levels, and thus a

more significant influence on the experimental results. As can be seen from Table 7, the order of ranges of the factors is water cut > emulsification temperature > salinity > stirring rate. Therefore, the water cut and emulsification temperature of the emulsion had the most significant influence on shear viscosity, followed by salinity, and finally stirring rate. In the subsequent experiments, the two factors with significant influences, water cut and emulsification temperature, were selected for single-factor studies.

Table 7. Orthogonal experimental results.

No.	Water Cut (%)	Emulsification Temperature (°C)	Stirring Rate (rpm)	Salinity (g/L)	Shear Viscosity (mPa·s)
1	1	1	1	1	18,297.6
2	1	2	3	2	18,601.8
3	1	3	2	3	24,229.3
4	2	1	3	3	13,417.6
5	2	2	2	1	12,753.7
6	2	3	1	2	16,840.5
7	3	1	2	2	1444.0
8	3	2	1	3	1070.9
9	3	3	3	1	1128.5
K1	61,128.6	33,159.2	36,209.0	32,179.9	
K2	43,011.8	32,426.5	38,427.1	36,886.3	
K3	3643.4	42,198.3	33,147.9	38,717.8	
k1	20,376.3	11,053.1	12,069.7	10,726.6	
k2	14,337.3	10,808.8	12,809.0	12,295.4	
k3	1214.5	14,066.1	11,049.3	12,905.9	
R	19,161.8	3257.3	1759.7	2179.3	

3.2.5. Effect of Water Cut on Oil–Water Emulsification

To investigate the effect of water cut on oil–water emulsification, emulsions were prepared using produced water from the YT Oilfield and heavy oil from Block A of the YT Oilfield at water cuts of 10%, 20%, 30%, 40%, and 50%, with the emulsification temperature controlled at 50 °C, the stirring rate at 750 rpm, and the emulsification time at 5 min. The shear viscosity at 50 °C was measured, and the results are listed in Table 8.

Table 8. Effect of water cut on the shear viscosity of emulsions at 50 °C.

Water Cut (%)	Shear Viscosity (mPa·s)		
	10 s^{-1}	30 s^{-1}	50 s^{-1}
10	7151.0	6517.3	6137.7
20	10,713.5	9395.1	8851.0
30	13,484.9	11,380.8	10,463.8
40	8657.3	7530.3	6834.4
50	2276.9	730.6	188.6

As can be seen from Table 8, at the same shear rate, the shear viscosity of the emulsions first increased and then decreased with increasing water cut. When the water cut was 10–30%, the shear viscosity was positively correlated with the water cut, reaching a maximum at 30%; this water cut was the phase inversion point. When the water cut was 30–50%, the higher the water cut, the lower the shear viscosity.

Before the phase inversion point, water is the dispersed phase in a W/O emulsion. As water cut increases, the droplet concentration and droplet–droplet interactions increase, and the total oil–water interfacial area increases. These effects raise the shear viscosity

until the inversion point. After the phase inversion point, the oil phase changed from the continuous phase to the dispersed phase, and the oil film could no longer encapsulate excess water droplets, forming a suspension system containing free water. Increasing the water cut increased the spacing between oil droplet molecules, weakened the internal forces of the oil–water system, and macroscopically manifested as a decrease in shear viscosity.

The water separation ratios of the emulsions after standing for 3 h at different water cuts are shown in Figure 7. At a water cut of 10%, the emulsion was very stable, and no free water separated out after standing for 3 h; therefore, only the water separation ratios for 20–50% are plotted in the figure. The stability order of the emulsions was 20% > 30% > 40% > 50%. At a water cut of 50%, the water separation ratio reached 96.5% within 0–0.5 h, and the increase was almost flat after 0.5 h, with a water separation ratio of 98.6% at 3 h. At a water cut of 40%, the water separation ratio increased most significantly within 0–1 h and slowed down after 1 h, with a water separation ratio of 57.7% at 3 h. At a water cut of 30%, the variation trend of the water separation ratio was similar to that at 40%, with a value of 55.4% at 3 h; water separated relatively quickly within 0–1.5 h and tended to level off after 1.5 h. At a water cut of 20%, the stability was significantly improved, with a water separation ratio of only 22.7% at 3 h. At low water cut, microscopy shows small, uniformly dispersed water droplets. The continuous oil phase and the interfacial film inhibit coalescence, so the emulsion remains stable and the water separation ratio is low. As water cut increases, droplets become larger and more closely packed, promoting coalescence and sedimentation under gravity, which increases the water separation ratio.

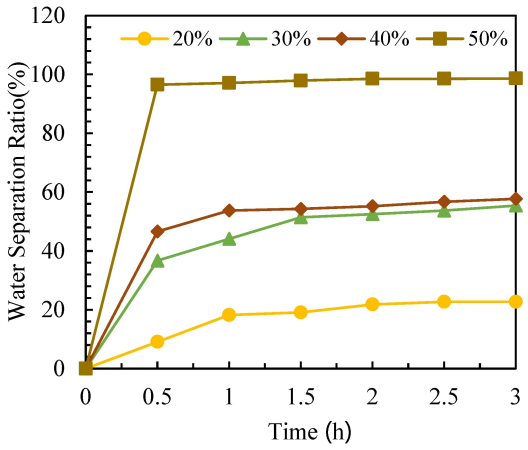
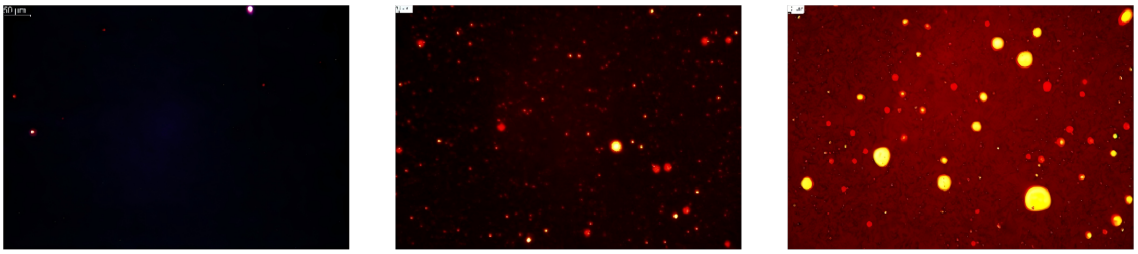


Figure 7. Water separation ratio of emulsions with different water cuts.

Figure 8 shows the microstructure of the emulsions at different water cuts. Because an unstable "water-floating-oil" type suspension formed after the phase inversion point, only the microstructure of W/O emulsions within the water cut range of 10–30% is recorded in the figure. At a water cut of 10%, the black oil phase accounted for the vast majority, with only a very small number of small water droplets scattered in the oil. At a water cut of 20%, the space occupied by the water phase increased significantly, the particle size of the small water droplets increased, and the distribution became denser and more compact. At a water cut of 30%, the water phase region further expanded, and the small water droplets micro-aggregated and coalesced into larger droplets with a more scattered distribution. The reasons are as follows: the higher the water cut, the more easily the water droplet aggregates collided and coalesced within the narrow space during mechanical stirring, forming droplets with larger particle sizes. The natural surface-active substances in the heavy oil tended to form an interfacial film at the oil–water contact surface under stirring. Before the interfacial film ruptured, increasing the emulsified water content allowed the oil

film to encapsulate more water droplet molecules, thereby increasing the area of the water phase region in the microstructure.



(a) 10% (b) 20% (c) 30%

Figure 8. Microstructure of W/O emulsions with different water cuts.

3.2.6. Effect of Emulsification Temperature on Oil–Water Emulsification

To investigate the effect of emulsification temperature on oil–water emulsification, a thermostatic water bath was heated to 40, 50, 60, and 70 °C, respectively. In each experiment, the mixture of heavy oil and produced water from the YT Oilfield was placed in the water bath for 10 min to reach the set temperature, and the emulsion was prepared at the set temperature with a water cut of 30%, a stirring rate of 750 rpm, and an emulsification time of 5 min. The shear viscosity of the emulsions at 50 °C was measured, and the results are listed in Table 9.

Table 9. Effect of emulsification temperature on the shear viscosity of emulsions at 50 °C.

Emulsification Temperature (°C)	Shear Viscosity (mPa·s)		
	10 s^{-1}	30 s^{-1}	50 s^{-1}
40	11,324.2	9059.9	8115.7
50	13,484.9	11,380.8	10,463.8
60	18,059.6	15,646.2	14,471.1
70	22,156.9	19,185.8	17,622.5

As can be seen from Table 9, at the same shear rate, the shear viscosity of the emulsions continuously increased with increasing emulsification temperature. When the emulsification temperature increased from 40 °C to 70 °C, the shear viscosity approximately doubled. The increase in viscosity with emulsification temperature is attributed to enhanced dissolution and adsorption of natural surfactants, a stronger interfacial film, and more complete emulsification, as supported by the microscopy results and previous studies [18]. The term 'surface activation energy' has been removed.

Figure 9 shows the variation in the water separation ratio of the emulsions with time at different emulsification temperatures. The order of the water separation ratio of the emulsions after standing for 3 h was 40 °C > 50 °C > 60 °C > 70 °C, indicating that the water separation ratio of the oil–water emulsions decreased with increasing emulsification temperature. The reasons are as follows: with increasing emulsification temperature, the solubility of natural surface-active substances in the crude oil in the oil–water emulsion increases. When the oil–water mixture is dispersed into small droplets under mechanical stirring, the surface-active substances adsorbed on the oil–water interfacial film are more sufficient, the emulsification effect is improved, and the formed oil–water interfacial film is stronger. Therefore, the stability of the emulsion is enhanced at higher temperatures, and the water separation ratio is reduced.

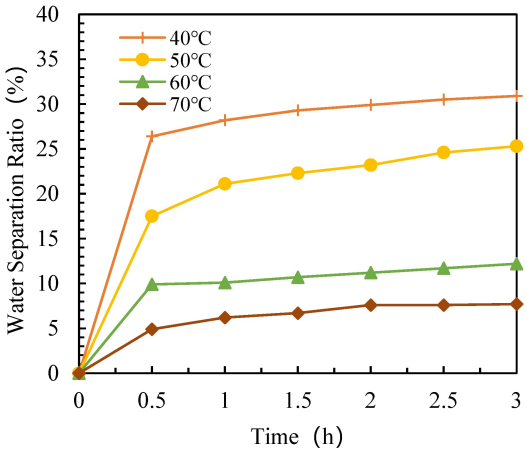


Figure 9. Water separation ratio of emulsions at different emulsification temperatures.

Figure 10 shows the microstructure of the emulsions at different emulsification temperatures. The emulsions were all W/O type at emulsification temperatures of 40–70 °C. At 40 °C, the number of droplets in the emulsion was relatively small, the distribution was sparse, and the spacing was large. With increasing emulsification temperature, the number of droplets in the W/O emulsion within the same field of view continuously increased, the droplets were more fully distributed in the heavy oil phase, the droplet spacing was significantly reduced, and the arrangement became denser. The temperature sensitivity of resins and asphaltenes promotes their dissolution in the light oil fraction and adsorption at the oil–water interface, strengthening the interfacial film and increasing the number of droplets. This is consistent with the microscopy results and previous studies on emulsification temperature and interfacial films [18,23].

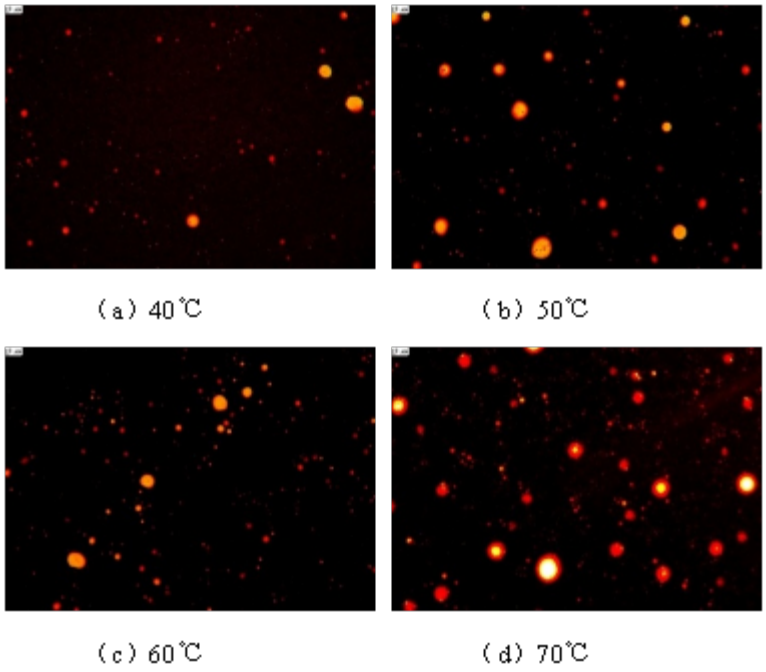


Figure 10. Microstructure of W/O emulsions at different emulsification temperatures.

3.3. Discussion of Mechanisms

Based on the physical properties of the heavy oil and the emulsification experiments, the phase inversion and stability of oil–water emulsions of heavy oil from Block A of the YT Oilfield are jointly controlled by internal and external factors. In terms of internal factors,

the total content of resins and asphaltenes in the heavy oil is approximately 40%. Resins, as natural surfactants, can adsorb at the oil–water interface to form an interfacial film with a certain strength, enabling the stable existence of W/O emulsions. Asphaltenes contain numerous fused-ring aromatic hydrocarbons and form high-strength hydrogen bonds with resins, increasing the viscosity of the oil phase and also enhancing the strength of the interfacial film. In terms of external factors, water cut, emulsification temperature, stirring rate, and salinity affect the shear viscosity and phase inversion point of the emulsions by changing the properties of the interfacial film, the droplet size and distribution, and the interaction forces between the oil and water phases.

Water cut is the most direct factor affecting phase inversion. At low water cut, the oil phase is the continuous phase and water droplets are dispersed in the oil. As the water cut increases, the probability of collision and coalescence of water droplets increases, the interfacial film area increases, and the shear viscosity rises. When the water cut exceeds the phase inversion point, the oil phase can no longer encapsulate the water droplets, and the system transforms into an O/W emulsion or a "water-floating-oil" suspension, causing a sharp decrease in shear viscosity. An increase in emulsification temperature improves the solubility of natural surfactants and the strength of the interfacial film, enabling the oil phase to encapsulate more water droplets and shifting the phase inversion point to a higher water cut. At the same time, the Brownian motion of droplets is enhanced at high temperatures, emulsification is more complete, the shear viscosity increases, and the static water separation ratio decreases. The stirring rate mainly affects the degree of droplet breakup and the accumulation of surface energy. It does not change the position of the phase inversion point but increases the shear viscosity at the phase inversion point. Salinity weakens the interfacial film through ionic electrical interference and the formation of metal soaps, making the emulsion more prone to separating free water and reducing the shear viscosity at the phase inversion point; however, under the experimental conditions, the position of the phase inversion point remained unchanged.

The orthogonal experiments showed that the order of influence of the factors was water cut > emulsification temperature > salinity > stirring rate. Therefore, in heavy oil gathering and transportation, controlling the water cut is the key to avoiding the formation of high-viscosity W/O emulsions. Although appropriately increasing the emulsification temperature can enhance emulsion stability, it also increases the shear viscosity; thus, a trade-off is needed between heating-induced viscosity reduction and emulsification-induced viscosity enhancement. Stirring rate and salinity can be used as auxiliary adjustment parameters.

4. Conclusions

In this study, heavy oil from Block A of the YT Oilfield was taken as the research object, and systematic tests of heavy oil physical properties and experiments on the phase inversion and stability of oil–water emulsions were carried out. The main conclusions are as follows:

(1) The heavy oil from Block A of the YT Oilfield behaved as a weakly non-Newtonian power-law fluid at 0 °C and 10 °C, showing slight dilatant characteristics at 0 °C and pseudoplastic behavior at 10 °C; at 20–60 °C, the flow behavior index was 1, indicating a Newtonian fluid. The consistency coefficient in the constitutive equation decreased continuously with increasing temperature, and the fitting correlation coefficients R^2 were all above 0.9.

(2) The heavy oil from Block A of the YT Oilfield had good temperature sensitivity. The viscosity decreased monotonically with increasing temperature. In the Newtonian region (20–60 °C), the Arrhenius fit gave an apparent activation energy of approximately 91.0 kJ/mol, characterizing the overall temperature sensitivity of viscous flow. The 0–10 °C weakly non-Newtonian behavior is reported separately, and no thermodynamic inflection

or structural transition is inferred from the linear μ − T plot. The density of the heavy oil decreased linearly with increasing temperature, with a density of approximately 0.96 g/cm^3 at 20 °C. The water cut was only 0.05%, so it could be regarded as anhydrous pure oil. Among the four fractions, the total content of resins and asphaltenes was about 40%, including 24.94% resins and 14.43% asphaltenes, which are important internal causes of the high viscosity and easy emulsification of the heavy oil.

(3) Before the phase inversion point of the oil–water emulsion, the shear viscosity increased with increasing water cut; after the phase inversion point, an unstable "water-floating-oil" suspension formed, and the higher the water cut, the lower the shear viscosity. An increase in emulsification temperature shifted the phase inversion point to a higher water cut and increased the shear viscosity at the phase inversion point. An increase in stirring rate did not change the phase inversion point but increased the shear viscosity at the phase inversion point. An increase in salinity did not change the phase inversion point but decreased the shear viscosity at the phase inversion point.

(4) Range analysis of the orthogonal experiments showed that the order of influence of the factors on the shear viscosity of the emulsions was water cut > emulsification temperature > salinity > stirring rate. Water cut and emulsification temperature were the main controlling factors affecting the phase inversion and stability of oil–water emulsification.

(5) The static water separation ratio of the emulsions increased with increasing water cut and decreased with increasing emulsification temperature. Microstructure observations showed that an increase in water cut increased the droplet size and expanded the water phase region, while an increase in emulsification temperature increased the number of droplets and made their distribution denser and arrangement more compact. The research results can provide an experimental basis for emulsification-based viscosity reduction, optimization of gathering and transportation processes, and phase inversion control of heavy oil in the YT Oilfield.

Author Contributions: All authors made substantial contributions to the manuscript. The manuscript was approved by all the authors. The authors did the following work: methodology, investigation, data curation, and writing—original draft, Z.W.; investigation, methodology, and supervision, H.C.; investigation and writing—original draft, L.D.; investigation, validation, and writing—review and editing, Y.F. All authors have read and agreed to the published version of the manuscript.

Funding: This program is financially supported by the Doctoral Research Start-up Fund of Jingchu University of Technology (Grant Nos. YYZ202637 and YYZ202636).

Data Availability Statement: Data available on request from the authors.

Conflicts of Interest: The authors declare no conflicts of interest.

Appendix A

Table A1. Replicate number and statistical analysis of emulsion experiments.

Experiment	Corresponding Figure/Table	Replicates (n)	Data Presentation	RSD	Statistical Method
Effect of water cut on shear viscosity	Table 8	3	Mean	3.0%	One-way ANOVA + Tukey's test ($p < 0.05$)
Effect of emulsification temperature on shear viscosity	Table 9, Figure 4	3	Mean	2.8%	One-way ANOVA + Tukey's test ($p < 0.05$)

Table A1. *Cont.*

Experiment	Corresponding Figure/Table	Replicates (n)	Data Presentation	RSD	Statistical Method
Effect of stirring rate on shear viscosity	Figure 5	3	Mean	3.2%	One-way ANOVA + Tukey's test ($p < 0.05$)
Effect of salinity on shear viscosity	Figure 6	3	Mean	3.5%	One-way ANOVA + Tukey's test ($p < 0.05$)
Water separation ratio at different water cuts	Figure 7	3	Mean	6.0%	One-way ANOVA + Tukey's test ($p < 0.05$)
Water separation ratio at different emulsification temperatures	Figure 9	3	Mean	5.5%	One-way ANOVA + Tukey's test ($p < 0.05$)
Orthogonal array $L9(3^4)$	Table 7	1 per run; central condition n = 3	Mean for repeated central condition	4.0% for central condition	Range analysis

References

1. Li, Q.; Wang, F.; Wu, J.; Li, Q.; Zhang, G. Multivariate coupling model and reservoir characteristics of enhanced geothermal reservoirs. *Energies* **2026**, *19*, 3180. [CrossRef]
2. Wu, J.; Li, Q.; Li, Q.; Wang, F.; Cheng, Y.; Yan, C. Design and optimization of bottom-hole temperature–pressure combinations in gas production from gas hydrates via carbon dioxide replacement strategy. *Energies* **2026**, *19*, 3536. [CrossRef]
3. Feng, A.; Li, Q.; Li, Q.; Wu, J.; Wang, F.; YanC. Numerical simulation investigation of fracture propagation behavior patterns and sensitivity factors of oil shale reservoirs in the Xunyi region considering the influence of natural fracture. *Geofluids* **2025**, *2025*, 2762142. [CrossRef]
4. Jiang, Q.; You, H.J.; Pan, J.J.; Wang, Z.Y.; Gai, P.Y.; Gates, I.; Liu, J.L. Preliminary discussion on current status and development direction of heavy oil recovery technology. *Spec. Oil Gas Reserv.* **2020**, *27*, 30–39.
5. Guo, Y.C. Research progress on heavy oil viscosity reduction methods. *Contemp. Chem. Ind.* **2019**, *48*, 155–158.
6. Yu, L.D. Distribution of world heavy oil resources and current status and prospects of recovery technologies. *Spec. Oil Gas Reserv.* **2001**, *8*, 98–103.
7. Wang, F.; Li, M.R.; Qi, L.Y. Study on correlation between polar four fractions of heavy oil and its viscosity and emulsion phase inversion point. *Chem. Eng. Oil Gas* **2013**, *42*, 637–641.
8. Tian, X.; Yu, P.; Wang, X.P.; Li, R.H.; Luo, A.J.; Chen, X.P.; Li, W.Y.; Yu, X.C.; Yu, L. Formation mechanism of water-in-oil emulsions in thermal recovery heavy oil in Liaohe Oilfield. *Sci. Technol. Eng.* **2026**, *26*, 1467–1476.
9. Ding, B.D.; Liu, L.; Zhang, W.L.; Gao, C.H.; Chen, X.W.; Guo, J.X. Research progress of emulsifying viscosity reducers for heavy oil. *Mod. Chem. Ind.* **2025**, *45*, 68–73.
10. Gong, J.; Dou, D. Prediction of shear viscosity of water-in-crude oil emulsions using an improved PR model. *J. China Univ. Pet. (Ed. Nat. Sci.)* **2007**, *31*, 114–118.
11. Meng, J.; Xiang, Y.; Wei, X.L.; Li, S.Y. Study on rheology of high internal phase water-in-heavy oil emulsions. *J. Southwest Pet. Univ.* **2007**, 122–124+191. Available online: https://kns.cnki.net/kcms2/article/abstract?v=qfSY-45OZzdZOHVBcvbmriQhYi39_U0omTMl992bek5Ayu_d30urds9bj4KCmtW_Ks2tbiU9MF9dJfotf0SqMsnylas_ElvH8LO5GGmTgAN7NIGx4WKrqSJKISVRZ4m9ZLY5r3PgQhQdc15gz9Wj7c09QL0Og-uBjzQJq48d7aeO_WiBWhNySw== (accessed on 20 October 2026).
12. He, W.Y.; Hao, Q.Y.; Li, M.R.; Meng, Q.Y.; Yu, G.S. Effect of temperature on water-cut inversion point and viscosity enhancement ratio of emulsified heavy oil. *J. Petrochem. Univ.* **2016**, *29*, 6–9.
13. Tian, M.C.; Jing, J.Q.; Wan, J.; Xie, Y.N.; Li, D. Experimental simulation of emulsification conditions for heavy oil–water two-phase flow. *Oil Gas Storage Transp.* **2012**, *31*, 250–253.
14. Gong, J.; Wang, W.; Yu, D. Experimental study on flow patterns of heavy oil–water two-phase flow in horizontal pipes. *Acta Pet. Sin.* **2007**, *28*, 140–143.
15. Lin, J.S.; Tang, P.Z.; Hao, Q.Y.; Li, M.R. Study on correlation between HLB value and water-cut inversion point of heavy oil. *Pet. Process. Petrochem.* **2015**, *46*, 61–65.

16. Wang, X.; Li, W.B.; Chen, X. Effect of preparation conditions on equilibrium shear viscosity of crude oil emulsions. *China Pet. Chem. Stand. Qual.* **2017**, *37*, 108–110. Available online: https://kns.cnki.net/kcms2/article/abstract?v=RyE_S26iMhVZ4MlW8oip0QlDPv7m2T46hAvryqpe1Akv1IW06GSBx3Y9w25DBHLTtknArH5zPkdhy4Q64BRuIpYWQaC5c0cRoeK4uMPPeRsJdSayPsfNQ2tfEDxTq4E1_un2gjkgWFo8ZvAsbE_T9wPo4mhnCDCxcFl7v3dZp7I=&uniplatform=NZKPT(accessed on 20 October 2026).
17. Chen, L.; Feng, C.; Ning, W.Y.; Zhang, K.X. Study on effects of external factors on stability of heavy oil emulsions. *Contemp. Chem. Ind.* **2014**, *43*, 691–693.
18. An, F.; Bai, J.; Qian, G.L. Study on stability of W/O emulsions of Liuhua heavy oil. *Petrochem. Equip.* **2013**, *16*, 19–22.
19. Sun, N.N.; Jing, J.Q.; Ding, Y.; Zang, X.X.; Zou, L. Effect of inorganic salt cations and anions on stability of O/W emulsions of heavy oil. *Chem. Ind. Eng. Prog.* **2015**, *34*, 3118–3123.
20. Ortiz, D.G.; Cambedouzou, J.; Bechelany, M.; Miele, P. Current trends in Pickering emulsions: Particle morphology and applications. *Engineering* **2020**, *6*, 468–482. [CrossRef]
21. Zhou, Q.X. Brief discussion on application of Stokes' law. *Mod. Educ.* **2019**, *6*, 230–232.
22. Luo, H.; Jia, Y.; Lu, Y.; Wen, J.; Luo, Y.; Wang, C.; Xiao, X.; He, Z.; Huang, Z.; You, C. Progress on Emulsification, Viscosity, Phase Inversion Characteristics, and Prediction Methods of Crude Oil–Water Mixed System. *ACS Omega* **2025**, *10*, 49321–49334. [CrossRef]
23. Al-Sakkaf, M.K.; Onaizi, S.A. Effects of emulsification factors on the characteristics of crude oil emulsions stabilized by chemical and Biosurfactants: A review. *Fuel* **2024**, *361*, 130604. [CrossRef]
24. Rafalscky, L.; Petroni, M.H.O.; Costa, T.R.S.; da Silva, M.; Siqueira, R.N.; Pegoretti, V.C.; Karnitz, O.; Oliveira, M.C.; Carvalho, R.M.; Chinelatto, L.S.; et al. Composition and stabilization mechanisms of interfacial material in petroleum emulsions: A systematic review. *Fuel* **2026**, *408*, 137763. [CrossRef]
25. Tang, L.; Wang, T.; Xu, Y.; Xu, M.; Wang, C. Research Progress on Demulsification Technology and Mechanism for Oilfield Crude Oil. *Energy Sci. Eng.* **2025**, *13*, 6572–6586. [CrossRef]
26. Ma, H.; Yang, D.; Li, Z.; Sun, Y.; Hu, Y.; Mao, X.; Lu, B.; Zhang, H.; Zeng, H. Probing the adsorption behavior and molecular interactions of asphaltene subfractions at Water–Toluene/Heptol interface. *Fuel* **2025**, *389*, 134577. [CrossRef]
27. Mahmoudi Alemi, F.; Mohammadi, S. Experimental Study on Water-in-Oil Emulsion Stability Induced by Asphaltene Colloids in Heavy Oil. *ACS Omega* **2025**, *10*, 14327–14342. [CrossRef]
28. *Standard's SY/T 0520-2008*; Determination of Crude Oil Viscosity: Rotational Viscometer Equilibrium Method. Standards Press of China: Beijing, China, 2008.
29. *Standard's GB/T 2540-1981*; Petroleum Products—Determination of Density (Pyknometer Method). Standards Press of China: Beijing, China, 1981.
30. *Standard's GB/T 260-2016*; Determination of Water Content in Petroleum Products (Distillation Method). Standards Press of China: Beijing, China, 2016.
31. *Standard's NB/SH/T 0509-2010*; Determination of Four Fractions in Petroleum Asphalt. Standards Press of China: Beijing, China, 2010.

Disclaimer/Publisher's Note: The statements, opinions and data contained in all publications are solely those of the individual author(s) and contributor(s) and not of MDPI and/or the editor(s). MDPI and/or the editor(s) disclaim responsibility for any injury to people or property resulting from any ideas, methods, instructions or products referred to in the content.